

Ray tracing of chemiluminescence in an unconfined non-premixed turbulent jet flame using large-eddy simulation

C.K. Ertem · J. Janicka · A. Dreizler

Received: 16 September 2011 / Revised version: 21 February 2012 / Published online: 21 April 2012
© Springer-Verlag 2012

Abstract Optical diagnostic techniques, such as chemiluminescence imaging, are commonly used to study turbulent flames. Inherent to turbulent flames is the spatio-temporal variation of the volumetric distribution of temperature and chemical composition. In consequence, the index of refraction varies accordingly and causes distortion of any optical ray intersecting the turbulent flame. This distortion is well known as beam steering. Beam steering may degrade imaging quality by reducing the overall spatial resolution. Its impact of course depends on the actual specifications of the imaging system itself. In this study a methodology is proposed to tackle this issue numerically and is exemplified for chemiluminescence imaging in a well-known turbulent hydrogen-fueled jet flame. Large-eddy simulation (LES) of this unconfined non-premixed flame is used to simulate instantaneous volumetric distributions of the flow and scalar fields including the local index of refraction. This simulation additionally predicts local concentrations of electronically excited chemiluminescent active species. At locations with significantly high concentrations of luminescent species, optical rays are initiated in the direction of the array detector used for recording single chemiluminescence images. Assuming the validity of geometrical optics, these rays are tracked along their pathways. Their direction of propagation changes according to the local instantaneous distribution of

the index of refraction. After leaving the computational domain of the ray tracing code which is fed by the LES, each ray is processed by the commercial code ZEMAX[®] and imaged onto an array detector. Measured and numerically simulated ensemble-averaged chemiluminescence images are compared to each other. Overall, a satisfying agreement is observed. The primary aim of this paper is the exposition of this method where numerical and experimental results are not any more compared in the flame but where this comparison is shifted to the imaging plane. Future extensions to higher pressures in enclosed combustors or internal combustion engines where beam-steering effects are much more pronounced than in atmospheric jet flames are addressed.

1 Introduction

Chemiluminescence measurements in turbulent flames are common practice within the combustion community, see for example [1–10]. Their passive nature compared to laser diagnostics makes chemiluminescence measurements much easier in their practical implementation. This particularly includes fewer requirements for an appropriate optical access and lower costs for instrumentation. The importance and the usability of the chemiluminescent light emissions and their possible relation to important measures such as heat release rate were investigated in one-dimensional flames experimentally by Haber et al. [9] including a chemical modeling approach. Moreover, the spatial intensity profiles of the chemiluminescent active species were simulated for two-dimensional laminar flames by Kojima et al. [10].

Floyd and Kempf [11] integrated chemiluminescence to an iterative computed tomography (CT) algorithm to retrieve the intensity field from images taken by multiple cameras positioned at varying positions around the flame. Using

C.K. Ertem · A. Dreizler (✉)
Center of Smart Interfaces, Institute of Reactive Flows
and Diagnostics, Technical University of Darmstadt, L1108
Petersenstrasse 32, 64287 Darmstadt, Germany
e-mail: dreizler@csi.tu-darmstadt.de

J. Janicka
Institute of Energy and Powerplant Technology, Technical
University of Darmstadt, L1101 Petersenstrasse 30, 64287
Darmstadt, Germany

this instrumentation, they studied the time-resolved three-dimensional information on various flame configurations in a simple and cheap way.

The industrial applicability of chemiluminescence for measurements of the fuel–air ratio also motivated researchers to investigate this method for internal combustion (IC) engines and gas turbine combustors [12–20]. Especially at high pressures and highly turbulent conditions, significant spatio-temporal variations of the index of refraction appear because of variations in local gas compositions and temperatures. In consequence, any optical rays will be steered such that chemiluminescence images recorded by array detectors such as CCD or CMOS cameras will be optically distorted. This distortion results in blurred images.

Quantification of such a blurring inherent to any optical diagnostic method applied to study turbulent combustion generally is not an easy task. The use of advanced instantaneous numerical simulation methods, such as large-eddy simulation (LES), allows deducing the spatial and temporal variations of the refraction-index fields in turbulent flames. Taking numerous instantaneous LES realizations, the corresponding fields of the index of refraction can be used subsequently for ray tracing purposes and for reconstructing the blurring in a statistical sense. Thereby, the limitation of imaging quality due to the transient nature of turbulent flames and aside of properties of the imaging system (lens and/or array detector) is quantified. However, such an evaluation does not allow any reconstruction of an unblurred instantaneous experimentally obtained image. It is noticeable that ray tracing is a post-processing step to individual LES realizations because the time scales of light propagation compared to typical time scales of turbulent flames are much smaller. Because of this feature, the proposed methodology can be easily adapted to any instantaneous flame simulation because of the absence of any feedback of light propagation to the flame simulation.

The scope of this paper is to present the newly developed numerical approach of determining optically blurred images caused by spatio-temporal variations of the index of refraction fields in turbulent flames. By this procedure, comparisons between numerically simulated and experimental results are moved to the imaging plane of the detection unit. Effects of beam steering are thereby accounted for in a statistical sense and any impact from this possible source of systematic errors when comparing experiments to simulations is reduced. This approach is exemplified for chemiluminescence imaging being a popular optical diagnostic technique in combustion research. However, the methodology can be extended to laser-based diagnostics where in addition to the optical distortion of the signal path, the laser beam entering the turbulent flame will also be affected by beam steering. Following a description of the procedure, the method is applied to a well-documented unconfined turbulent non-premixed hydrogen-fueled jet flame. Measured and

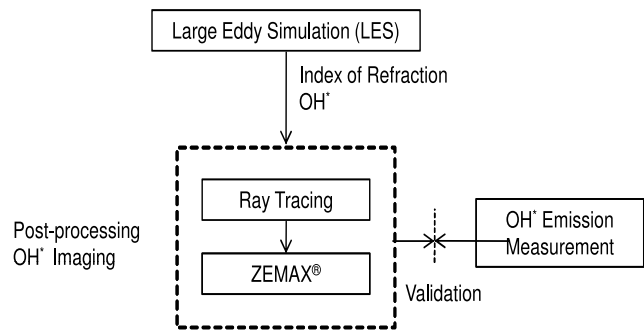


Fig. 1 Flowchart of the chemiluminescence imaging method

numerically simulated chemiluminescence images are compared to each other, showing the potential of the method.

2 Chemiluminescence imaging method

The main tools used for the chemiluminescence imaging are the program FLOWSI for the large-eddy simulation, an extended model for combustion containing the chemiluminescent species (here electronically excited OH^* emitting in the spectral range around 310 nm) [21, 22] included to the LES approach, a ray tracing code (RTC) and the optical design software ZEMAX[®] for proper modeling of the telephoto lens used for imaging the chemiluminescence. The programs FLOWSI and RTC are in-house-developed codes whereas ZEMAX[®] is a commercial program. The interfaces between the different codes and the exchanged information are shown schematically in Fig. 1. Instantaneous realizations of the combustion LES provide information on local concentrations of the luminescent species (OH^*) and the corresponding volumetric distribution of the index of refraction n . Rays from those volume elements containing substantial OH^* concentrations are initiated in the direction of the intensified CCD camera and propagate through the turbulent flame. In general, the individual beam directions will be changed due to beam steering. After leaving the LES domain, each single beam is imaged onto the array detector using ZEMAX[®]. More details are provided in the following subsections.

2.1 Large-eddy simulation

For the large-eddy simulation (LES) of the unconfined non-premixed flame, the in-house code FLOWSI in connection with tabulated chemistry is used; for more comprehensive details see Forkel and Janicka [23], Kempf et al. [24] and Flemming et al. [25]. As only the mixture fraction is transported in this very common LES approach, the local OH^* concentrations are deduced from look-up tables interlinking the mixture fraction and the luminescent species concentrations [26, 27]. The laminar opposed jet calculations

for the look-up tables are performed prior to the LES using Chem1D provided by Somers [28]. The underlying chemical model includes electronically excited luminescent species adding to the number of species in the original detailed reaction mechanism (GRI-Mech 3.0). Generation and destruction of the electronically excited species are described in appropriate elementary reactions and are taken from Kathrotia et al. [21]. Because hydrogen was used as fuel, in this study the only relevant electronically excited luminescent specie is OH*. However, inclusion of other luminescent species important for combustion of hydrocarbon-based fuels such as CH* is equally possible.

Turbulence–chemistry interaction is modeled with a presumed PDF (probability density function) method taken from Janicka and Kollmann [29]. The Smagorinsky model and dynamic determination of model coefficients using the Germano procedure [30] are applied. The simulated time-dependent OH* concentrations and refraction-index fields n from the combustion LES are used subsequently in post processing as input data for the ray tracing code (RTC).

For instantaneous realizations of flow and scalar fields obtained by LES, the local OH* concentrations are normalized to the maximum concentration observed in the look-up tables. For each volume element that exhibits normalized OH* concentration exceeding a user-defined threshold, a fixed number of optical rays are initiated. Restricting the present analysis to domains of maximum heat release and to minimize the computational costs, the threshold used here is 0.1. Each ray is weighted by the normalized OH* concentration of its origin. Directions of the rays are varied randomly within the angle of observation.

Following their initiation, each single ray is tracked through the instantaneous scalar field (see Sect. 2.2). The spatial and time-dependent variations of the index of refraction n result from the local gradients within the turbulent flame and cause varying deflections for all different LES realizations. In other terms, the deflection of the chemiluminescence signal is determined by changes of both temperature and chemical composition throughout the flame. As presented by Gardiner et al. [31], the index of refraction can be calculated from the Lorentz–Lorenz equation

$$n = \left(\frac{RT/p + 2\langle R_L \rangle}{RT/p - \langle R_L \rangle} \right)^{1/2}, \quad (1)$$

where R , T and p denote the ideal gas constant, temperature and pressure, respectively. The average molar refractivity $\langle R_L \rangle$ may be computed for a gas containing S species from

$$R_L = \sum_{i=1}^S R_{Li} X_i, \quad (2)$$

where X_i is the mole fraction and R_{Li} the molar refractivity of the species i [31]. The local species concentration

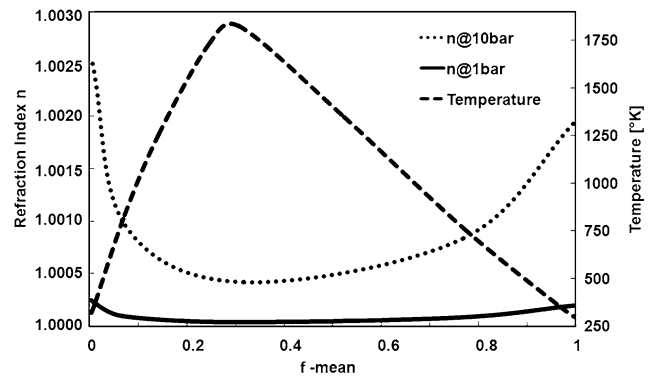


Fig. 2 The temperature T and refraction index n shown as functions of the mixture fraction for a diffusion flamelet. Temperature is shown for atmospheric conditions

is deduced from the local mixture fraction using the aforementioned look-up tables. In Fig. 2, the index of refraction as a function of the mixture fraction is shown exemplarily for a laminar flamelet calculation at a constant strain rate of $a = 30 \text{ s}^{-1}$. The difference between the continuous line representing the index of refraction for atmospheric conditions and the dotted line representing the index of refraction at 10 bar shows the ascending importance of beam-steering effects with increasing pressure. For this reason, optical diagnostics applied to practical combustion geometries operated at elevated pressures such as IC engines or gas turbine combustors will be affected much more than atmospheric flames. However, this study introduces the new methodology of treating beam-steering effects in comparisons of numerical and experimental results. The transfer to high-pressure applications is beyond the scope of this paper.

2.2 Ray tracing

A key result from the combustion LES for ray tracing of chemiluminescence as a post-processing step are the instantaneous discrete volumetric refraction index fields. For ray tracing, however, continuous distributions of the refraction index are required. For this purpose, one needs an accurate volumetric reconstruction. Here we propose a tricubic interpolation that fulfills the requirement of being continuously differentiable in all three spatial coordinates.

The wavelength λ of the chemiluminescence signal is much smaller compared to the resolved characteristic scales of the reactive flow. For this reason, the principles of geometrical optics are decisive for beam-steering effects and wave characteristics of light, e.g. interference and diffraction, are neglected in the flame. Thus, one can use Fermat's law to describe mathematically the propagation of light rays through the simulated refraction-index field by using the concept of minimization.

In the inhomogeneous medium, the index of refraction varies as a function of the position $n(\mathbf{r})$. Therefore, the op-

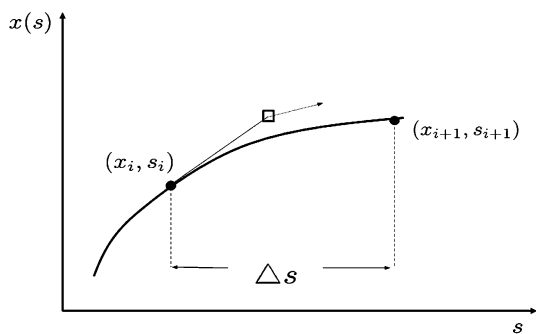


Fig. 3 Schematic illustration of the one-dimensional ray propagation, where s denotes the ray path, (x_i, s_i) the originating point of the ray and the hollow square a substep point of the Runge–Kutta scheme

tical length \mathcal{L} or the eikonal, which is the traversed path in least time, is written as

$$\mathcal{L}_{\min} = \int_{\mathcal{T}} n(\mathbf{r}) \, ds \tag{3}$$

and the contribution of an infinitesimal path ds along a trajectory \mathcal{T} to \mathcal{L}_{\min} is

$$d\mathcal{L}_{\min} = n \, ds = n \mathbf{e}_t \cdot d\mathbf{r} = \nabla \mathcal{L}_{\min} \cdot d\mathbf{r} \tag{4}$$

with $\mathbf{e}_t = d\mathbf{r}/ds$ being the tangential unit vector of the trajectory and with the interrelation

$$n^2 = (\nabla \mathcal{L}_{\min})^2 \tag{5}$$

known as the eikonal equation. Following the procedure of Meschede [32], in the next steps the equation is differentiated and rewritten to obtain the following form:

$$\frac{d}{ds} \left(n \frac{dx_i}{ds} \right) = \frac{\partial n}{\partial x_i} \tag{6}$$

In order to solve Eq. (6) numerically, it is still necessary to rewrite the eikonal. This last step leads to three differential equations for the three spatial directions x , y and z . Shown exemplarily for one dimension, the equation in the x -axis direction reads

$$n \frac{d^2x}{ds^2} = \frac{\partial n}{\partial x} - \frac{dx}{ds} \left(\frac{\partial n}{\partial x} \frac{dx}{ds} + \frac{\partial n}{\partial y} \frac{dy}{ds} + \frac{\partial n}{\partial z} \frac{dz}{ds} \right) \tag{7}$$

A Runge–Kutta fourth-order scheme has been used and proven its suitability for numerical ray tracing in gradient-index media in previous works by Puchalski [33]. To simulate the propagation of the chemiluminescence signal, the eikonal equation (7) is numerically solved for the three spatial directions separately. Figure 3 illustrates a schematic sketch of a ray path solved in Eq. (7).

Since the distribution of the index of refraction is not known as a continuous function of position but as a discrete distribution resulting from the LES, interpolating the partial

derivative $\partial n/\partial x_i$ where $i = 1, 2, 3$ is not appropriate. Instead, the tricubic engine is chosen which is a local tricubic interpolation scheme (local third-order polynomial in three-dimensional space) in three dimensions as detailed in [34]. The important advantage of this method is that the function $n(x, y, z)$ and its first derivatives in the x, y, z directions are continuous. The outcome of this tricubic interpolation scheme is the volumetric distribution of the refraction index $n(x, y, z)$ that is represented by the following function:

$$n(x, y, z) = \sum_{i=0}^3 \sum_{j=0}^3 \sum_{k=0}^3 a_{ijk} x^i y^j z^k \tag{8}$$

The coefficients a_{ijk} are stacked in a vector \mathbf{a} in such a way that the conditions of continuous differentiability mentioned above are satisfied. The vector \mathbf{a} is composed of 64 entries. They are computed with a linear relationship $\mathbf{a} = B^{-1}\mathbf{b}$, where \mathbf{b} contains the constraints on n and its derivatives. The 64×64 matrix B has only integer entries and its inverse is provided by Lekien and Marsden [34].

The ray tracing code was checked to accurately reproduce important features such as refraction or the reversibility of light arising from Fermat’s law.

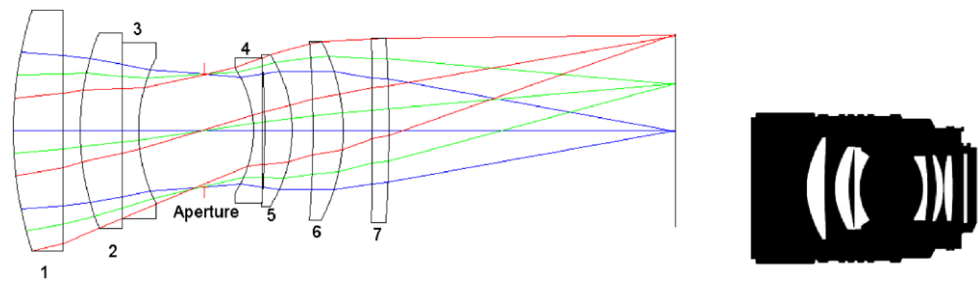
2.3 Design of the objective lens

For chemiluminescence imaging commercial objectives are commonly used in connection with intensified CCD cameras. Such objectives are advantageous compared to single lenses because the aperture and thereby the depth-of-field can be easily adjusted to the needs of the individual experimental conditions. To more appropriately account for the actual imaging properties of an objective than possible by ray optics, its properties are simulated by the commercial software ZEMAX®. However, the general difficulty is that no ZEMAX® models of standard objectives are accessible to the public. For this reason, the objective used in the present experiments is redesigned.

In the present study a UV-transmissive AF DC-Nikkor 105 mm $f/4.5$ telephoto lens is used. As mentioned, the objective is redesigned using the commercial software ZEMAX® [35] and taking advantage of information on Nikkor 105 mm objectives accessible to the public [36]. For redesign purposes, the ‘sequential mode’ available within ZEMAX® is used. In sequential mode, the rays intersect each surface only once without being reflected or refracted. The number of elements in the designed objective lens is seven and the aperture is positioned in between elements 3 and 4 (see Fig. 4).

For the redesign of the objective lens, the focal length ($f = 105$ mm), the aperture ($f/4.5$), the maximum angle of field of view (12°) and the modulation transfer function (MTF) are benchmarks within the ZEMAX® model. Unfortunately, it is not known for which specific wavelength the

Fig. 4 Layout of designed objective lens (*left*) and layout provided by Nikon (*right*)



MTF provided by Nikon [36] is valid. For this reason, an optimization of the present design is done by varying the wavelength using three common wavelengths of $\lambda_1 = 486$ nm, $\lambda_2 = 587$ nm and $\lambda_3 = 656$ nm.

In the final redesigned objective, the MTF provided by Nikon is matched up to approximately 35 line pairs per mm. In this context, this is judged as sufficiently good. Compared to the real objective lens, the redesigned lens is shorter by 4 mm. This causes a relatively small change in aperture by approximately 10 %. On the other hand, the focal length of $f = 105$ mm and the maximum angle of field of view (12°) are matched very well.

Notice that for the actual simulation of the chemiluminescence images, ZEMAX[®] is operated in its ‘non-sequential mode’ where reflection and refraction are taken into account. Thereby, blurring due to Fourier optics is considered for the simulation of chemiluminescence imaging.

3 Experimental test case and numerical setup

The numerical chemiluminescence imaging method consisting of LES using tabulated chemistry (FLOWSI), ray tracing (RTC) and lens simulation (ZEMAX[®]) is applied to the H3 flame, a turbulent non-premixed jet flame investigated within the framework of the TNF Workshop [37, 38]. The H3 flame consists of a central fuel jet (inner diameter $D = 8$ mm) of 50/50 vol% H_2/N_2 with a stoichiometric mixture fraction of $f_{st} = 0.31$. The bulk velocity of the fuel jet is $U_{jet} = 34.8$ m/s resulting in a jet exit Reynolds number of $Re \approx 10000$ based on the fuel properties and the jet nozzle diameter. A large coannular air nozzle surrounds the central jet and supplies a laminar flow with an axial velocity of 0.2 m/s. The gases at the inflow boundary are at ambient temperature of 294 K.

Luminescence of the electronically excited OH^* radicals is imaged by the aforementioned DC-Nikkor 105 mm objective onto an intensified CCD camera (Roper) operated in its linear regime. By means of an interference filter placed in front of the objective, only OH^* chemiluminescence around 310 nm is recorded. An aperture is used similar to the ZEMAX[®] model described in the previous section. The working distance measured from the jet center line to

the entrance plane of the objective is 710 mm resulting in a collection angle of 0.075 rad in both directions. Using short exposure times, instantaneous realizations of the chemiluminescence are measured for a subsequent statistical comparison with simulation results. Comparisons are based on relative but not absolute OH^* -chemiluminescence intensities. Thus, cumbersome calibration procedures are avoided. To obtain relative OH^* -chemiluminescence intensities from the experiments, the highest luminosity intensity observed at an axial distance at $x/D = 1$ is used. This choice is justified because at this axial height only insignificant radial fluctuations are apparent. Images are background corrected and normalized prior to the calculation of the ensemble average. Measurements are restricted to an area spanning from $x/D = 0$ to 40. Chemiluminescence is measured in eight axial consecutive segments. For each segment, 250 single camera exposures are recorded.

The LES has been performed on a staggered cylindrical grid consisting of $512 \times 32 \times 67 \approx 5 \times 10^5$ cells in axial, circumferential and radial directions, respectively. The complete domain has a physical size of $0.512 \times 2\pi \times 0.18$ m³. The nozzle is extended one diameter into the surrounding coflowing air to allow for shear-generated velocity fluctuations directly at the nozzle exit. Spatially and temporally varying OH^* concentrations are normalized to the maximum OH^* concentration in the look-up tables (compare Sect. 2.1).

The ray tracing code (RTC) is performing on a collocated equidistant Cartesian grid consisting of $240 \times 60 \times 60$ cells in x , y and z directions, respectively, and a constant grid spacing of $x_i = 0.001$ m in all directions. The x coordinate is aligned with the axis of the cylindrical grid and the origin is located at $(x_0; r_0) = (0.01; 0.00)$ m. For saving computational time of the post processing, a reduced domain of $30D \times 7.5D \times 7.5D$ is used for the chemiluminescence signal post processing.

4 Results and discussion

For an evaluation of the simulation results and their comparison to experimental findings, approximately 1500 statistically independent samples of the flow and scalar fields have been extracted from the LES over a period of 0.15 s real

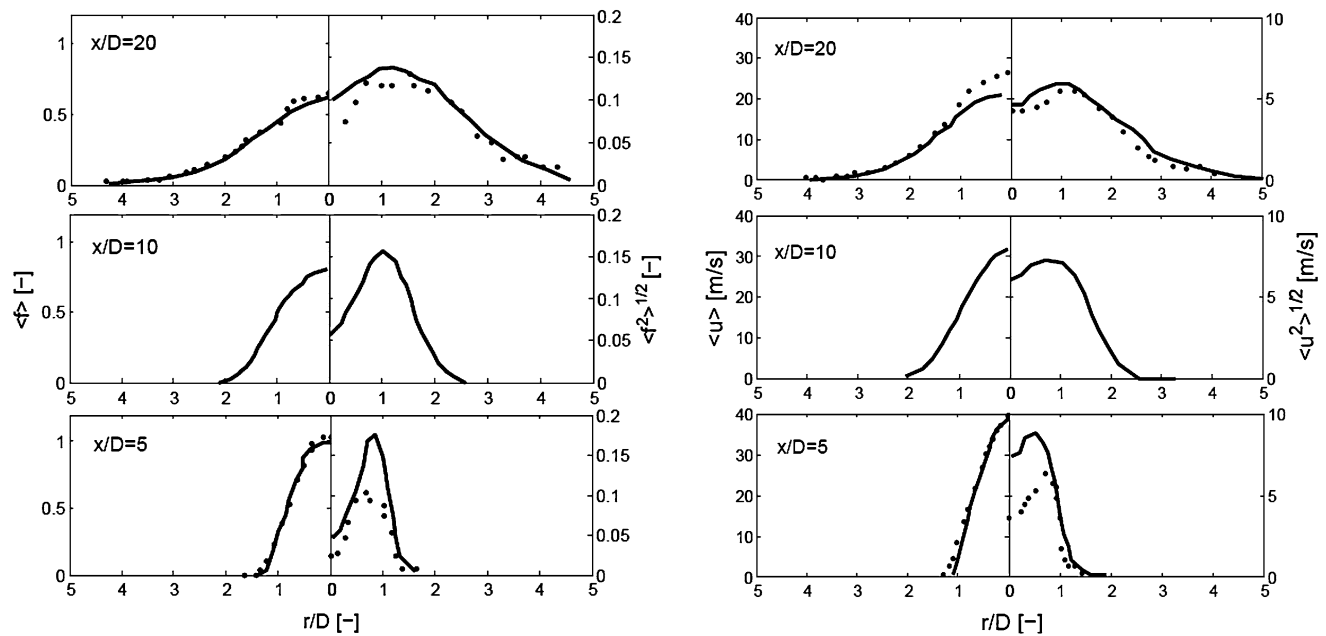


Fig. 5 Radial distributions of mixture fraction (*left*) and axial velocity (*right*) statistics for the H3 flame. The *dots* show the experimental data and the continuous line the LES data

time. The results are presented in a non-dimensional form using the nozzle diameter D and normalization to the maximum chemiluminescence intensity as described in the previous sections.

Measured [37] and numerically simulated distributions of the mixture fraction and the axial velocity component are compared in Fig. 5 showing radial profiles at some selected axial heights. It can be deduced that the spreading rate of the flame is captured reasonably well. Additionally, the level of fluctuations is in agreement with the experimental findings at least for axial locations above $x/D = 5$. This confirms that intermittent structures in the shear layers of the flame are predicted in accordance with the experiment. This overall good agreement between LES and experimental results is a prerequisite for using the instantaneous scalar fields for a numerical simulation of the chemiluminescence by OH^* radicals.

The right-hand side of Fig. 6 shows the normalized ensemble-averaged chemiluminescence images reconstructed from 250 individual images measured at each of the eight consecutive segments along the axial extension of the flame. Chemiluminescence from the electronically excited OH^* radicals is restricted to the mean reaction and heat release zone around the stoichiometric mixture fraction. This is caused by its short upper-state lifetime (few ns at atmospheric conditions) due to intermolecular collisions and the spatially narrow region of OH production. At low axial heights up to approximately $x/D = 5$, the reaction zone shows only very little intermittency. Therefore, the chemiluminescence exhibits in the radial direction a pronounced

intensity maximum around $r/D = 0.5$. Because chemiluminescence imaging is a line of sight method the inner part of the jet flame shows as well some luminosity but obviously at a much lower intensity level. For increasing axial heights the flame spreads in the radial direction. The profiles of mixture fraction and velocity distribution become wider. Accordingly, the mean reaction zone becomes wrinkled and highly intermittent. Chemiluminescence appears consequently at various locations and ensemble-averaged images exhibit a significantly extended chemiluminescence profile in the radial direction. The peak intensities drop to below 0.4 at an axial height of $x/D = 25$.

Notice that flame spreading entails extended radial dimensions of the flame at progressively downstream locations. This feature increasingly causes additional blurring because chemiluminescence originating from areas displaced from the focal plane of the detection unit is more and more out of focus. In a chemiluminescence imaging experiment, this is unavoidable and depends on the choice of various experimental components and parameters. Within the present simulation, these effects are accounted for but so far no efforts were undertaken to separate these different causes for blurring.

At the left-hand side of Fig. 6 ensemble-averaged radial profiles of measured chemiluminescence are compared to simulation results for axial heights spanning from $x/D = 5$ to 25 in increments of 5. The decrease of the relative peak intensity with increasing height is captured very well. However, the radial location of the peak intensity is displaced closer to the jet center line for the simulated profiles. This

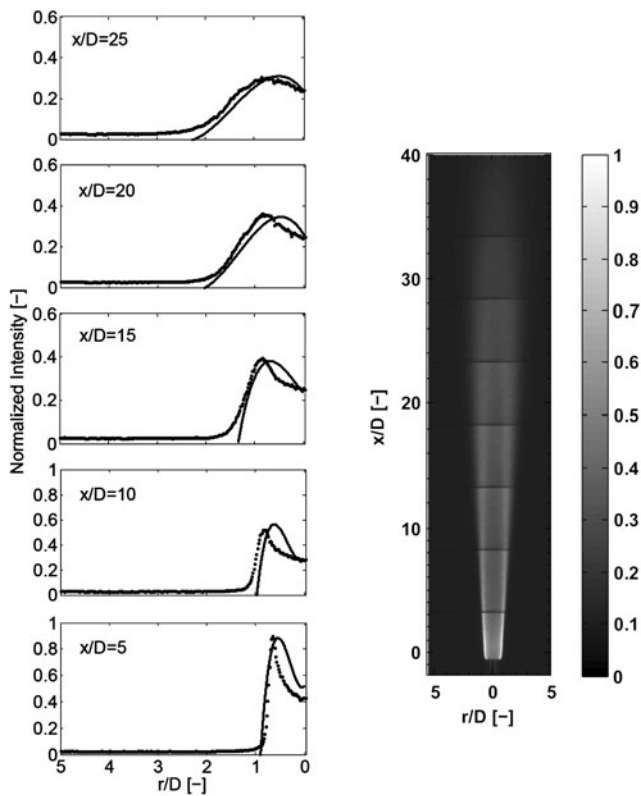


Fig. 6 *Right-hand side*: mean image of the chemiluminescence measurement of H3 flame normalized to its maximum intensity. *Left-hand side*: ensemble-averaged normalized chemiluminescence signal intensity. The *dotted line* shows the experimental data and the *continuous line* represents the simulated data

offset is observed already at $x/D = 5$ and increases slightly for increasing axial heights. Different reasons might cause this mismatch. At first, the spreading rate of the flame and correspondingly the radial extension of the mean reaction zones (stoichiometric contours) might be underpredicted. Despite the remaining differences between measured and simulated mixture fraction profiles obvious from Fig. 5, this possibly is not the most obvious reason. Second, the radial offset might be partly produced from an imperfect model of the objective such that out-of-focus contributions in the simulations contribute differently to the chemiluminescence image than in reality. As a third possibility, it is speculated that optical blurring is underpredicted because of insufficient spatial variations of the index of refraction field. As LES solves filtered conservation equations subgrid variances are modeled; because the lack of an appropriate model the volumetric distribution of the index of refraction in the present approach is reconstructed from the resolved part of the scalar field only. In turn, variations of the refraction index at the subgrid level are not captured. However, with increasing axial height, length scales of the flame increase and LES grid resolution should become less of an issue. Further downstream one would expect for this reason a reduced ra-

dial displacement between measured and simulated intensity peaks. As this is not clearly evident from the profiles shown in Fig. 6, this issue remains unresolved in the present study. Sensitivity studies based on grid refinement are one option to investigate the contributions to beam steering at a subgrid level more thoroughly.

In contrast to the measurements, simulated chemiluminescence profiles exhibit a sharp cut-off at their outer edges. Similarly for axial heights above $x/D = 15$ a non-zero gradient is observed at the center line. Reasons for this non-physical behavior are not yet completely clear. In future research, conceivable influences upon simulated radial profiles of chemiluminescence should be addressed, such as flame intermittency, the initiation of optical rays and clipping chemiluminescence below a user-defined threshold.

5 Conclusions

Beam steering is inherent to optical diagnostics when applied to study turbulent flames. Beam steering is caused by spatio-temporal variations of the volumetric distribution of the refraction index, which is dependent on local gas composition and temperature. If beam steering appears at significant levels, the imaging quality can be limited due to optical blurring and not any more by restrictions of the telephoto lens and/or array detector. In general, beam-steering issues increase in their significance for high turbulence levels and high combustion pressures apparent in practical applications such as IC engines or gas turbine combustors. There is no obvious way to reconstruct individually blurred single-shot images recorded by any optical diagnostic method. However, in a statistical manner a comparison between measured and numerically simulated turbulent flames might be improved when ray tracing is included to the numerical simulation. In this sense the plane where comparisons between experiments and simulations are performed is shifted to the array detector.

Following this idea, this paper discusses an approach based on large-eddy simulation (LES) and tabulated chemistry. LES emerged in the last decade to become a reliable tool for simulating instationary turbulent flames. Using chemiluminescence imaging as a widely used optical measuring technique, the detailed chemistry mechanism underlying the tabulation is extended by inclusion of elementary reactions describing the generation and destruction of chemiluminescent active species. As here a hydrogen-fueled flame is considered, the only relevant chemiluminescent species is electronically excited OH^* emitting around 310 nm. For instantaneous LES realizations the locations of significant OH^* concentrations are identified. From these locations, rays are initialized with directions randomly varied within the solid angle of detection. The propagation through

the turbulent flame towards the detector is modeled by taking into account the local distribution of the index of refraction that is dependent on the local mixture fraction and similarly tabulated as all other scalars. Following the LES domain, the rays with differing angles are imaged onto the plane of the array detector using the commercial program package ZEMAX[®]. For this purpose, the telephoto lens used in the experiments is modeled matching important features that are accessible to the public.

The performance of this modeling approach is evaluated by comparing measured and simulated chemiluminescence images. For this purpose, a well-documented turbulent non-premixed hydrogen-fueled jet flame is used. For this flame, significant experience in terms of LES exists and reliable scalar as well as velocity field data are accessible. The comparison is made using normalized chemiluminescence images in order to prevent a cumbersome calibration process. Overall, a reasonable agreement between measured and simulated chemiluminescence images is obtained. Whereas the drop of the maximum intensities with increasing axial heights is reproduced, the peak location in the radial direction is not so well captured. Although minor differences in the radial location of the mean reaction zones are observed, other reasons most likely cause these deviations. It is hypothesized that subgrid fluctuations of the refraction index that are not yet captured in the present LES approach may be one of the reasons for these deviations. Further investigations are needed to more closely examine this issue. A sensitivity study with respect to the grid resolution might be one way to quantify the impact of the unresolved part. As a result, a subgrid model for the refraction index might be needed. Furthermore, the proposed methodology might be extended for inclusion of radiation trapping using local concentrations of OH radicals in their electronic ground states. As this paper introduces a new methodology comparing measured and simulated turbulent flames, however, these issues are beyond the scope of the study and remain open for further investigation.

Acknowledgements The authors gratefully acknowledge the sponsorship of the Deutsche Forschungsgemeinschaft (contract no. DFG JA 544/35-2).

References

- M. Lauer, T. Sattelmayer, in *VDI Flammentag*, vol. 23, Berlin (2007)
- M. Lauer, T. Sattelmayer, *Appl. Phys. B* (2012 in press)
- M. Bozkurt, M. Hartmann, T. Kathrotia, U. Riedel, M. Fikri, C. Schulz, in *4th Eur. Combustion Meet.* (2009)
- M. Röder, T. Dreier, C. Schulz, *Appl. Phys. B* (2012 in press). doi:10.1007/s00340-012-4990-0
- M.K. Chin, J.D. Smith, V. Sick, *SAE Int. J. Fuels Lubr.* **1**, 570 (2008)
- C.M. Fajardo, J.D. Smith, V. Sick, *J. Phys. Conf. Ser.* **45**, 19 (2006)
- U. Fissenewert, V. Sick, H. Pucher, *SAE Trans. J. Fuels Lubr.* 786 (2005)
- J.D. Smith, V. Sick, *Appl. Opt.* **44**, 6682 (2005)
- L.C. Haber, U. Vandsburger, W.R. Saunders, V.K. Khanna, *Proc. IGTI* **121**, 1 (2000)
- J. Kojima, Y. Ikeda, T. Nakajima, *Combust. Flame* **140**, 34 (2005)
- J. Floyd, A.M. Kempf, *Proc. Combust. Inst.* **33**, 751 (2011)
- T. Chou, D.J. Patterson, *Combust. Flame* **101**, 45 (1995)
- P.G. Aleiferis, T. Hardalupas, A.M.K.P. Taylor, K. Ishii, Y. Urata, *Combust. Flame* **136**, 72 (2004)
- Y. Hardalupas, C.S. Panoutsos, A.M.K.P. Taylor, *Exp. Fluids* **49**, 883 (2010)
- Y. Hardalupas, M. Orain, *Combust. Flame* **139**, 188 (2004)
- M. Orain, Y. Hardalupas, C. R., *Méc.* **338**, 241 (2010)
- C.S. Panoutsos, Y. Hardalupas, A.M.K.P. Taylor, *Combust. Flame* **156**, 273 (2009)
- P. Kutne, R. Sadanandan, W. Meier, in *4th Eur. Combustion Meet.* (2009)
- B. Ayooola, R. Balachandran, J. Frank, E. Mastorakos, C. Kaminiski, *Combust. Flame* **144**, 1 (2006)
- F. Güthe, B. Schuermans, *Meas. Sci. Technol.* **18**, 1 (2007)
- T. Kathrotia, U. Riedel, J. Warnatz, in *4th Eur. Combustion Meet.* (2009)
- T. Kathrotia, U. Riedel, A. Seipel, K. Moshhammer, A. Brockhinke, *Appl. Phys. B* (2012 in press). doi:10.1007/s00340-012-5002-0
- H. Forkel, J. Janicka, *Flow Turbul. Combust.* **65**, 163 (2000)
- A. Kempf, F. Flemming, J. Janicka, *Proc. Combust. Inst.* **30**, 557 (2005)
- F. Flemming, A. Sadiki, J. Janicka, *Proc. Combust. Inst.* **31**, 3189 (2007)
- N. Peters, *Proc. Combust. Inst.* **21**, 1231 (1986)
- R.W. Bilger, S.H. Stårner, R.J. Kee, *Combust. Flame* **80**, 135 (1990)
- B. Somers, The simulation of flat flames with detailed and reduced chemical models, Dissertation, Technische Universiteit Eindhoven, 1994
- J. Janicka, W. Kollmann, *Proc. Combust. Inst.* **17**, 421 (1978)
- M. Germano, U. Piomelli, P. Moin, W. Cabot, *Phys. Fluids A* **3**, 1760 (1991)
- W.C. Gardiner Jr., Y. Hidaka, T. Tanzawa, *Combust. Flame* **40**, 213 (1981)
- D. Meschede, *Optik, Licht und Laser* (Teubner, Stuttgart, 1999) Chap. 1
- J. Puchalski, *Appl. Opt.* **33**, 1900 (1994)
- F. Lekien, J. Marsden, *Int. J. Numer. Methods Eng.* **63**, 455 (2005)
- ZEMAX[®] Optical Design Program User's Guide (2008)
- <http://imaging.nikon.com/lineup/lens/singlefocal>, © 2011 Nikon Corporation
- R. Barlow (ed.), *Proc. TNF Workshops* (2012). <http://www.sandia.gov/TNF/abstract.html>
- D.G. Pfuderer, A.A. Neuber, G. Früchtel, E.P. Hassel, J. Janicka, *Combust. Flame* **106**, 301 (1996)